Testing the radiometric accuracy of Fourier transform infrared transmittance measurements

S. G. Kaplan, L. M. Hanssen, and R. U. Datla

We have investigated the ordinate scale accuracy of ambient temperature transmittance measurements made with a Fourier transform infrared (FT-IR) spectrophotometer over the wavelength range of 2–10 μm. Two approaches are used: (1) measurements of Si wafers whose index of refraction are well known from 2 to 5 μm, in which case the FT-IR result is compared with calculated values; (2) comparison of FT-IR and laser transmittance measurements at 3.39 and 10.6 μm on nominally neutral-density filters that are free of etaloning effects. Various schemes are employed to estimate and reduce systematic error sources in both the FT-IR and laser measurements, and quantitative uncertainty analyses are performed.

Key words: Fourier transform infrared spectrophotometer, neutral-density filter, transmittance, photometric accuracy.

1. Introduction

Fourier transform infrared (FT-IR) spectrometers have become the most popular and commonly used instruments for the spectral characterization of materials in the infrared. Their well-known advantages in throughput and signal averaging,[1] combined with advances in high-speed computing for real-time phase correction and Fourier transform processing, and clever engineering of dynamically stabilized moving mirror systems, have led to commercially available systems that are capable of unprecedented speed, signal-to-noise ratio, and stability. These devices have now largely supplanted dispersive instruments for transmittance, reflectance, absorptance, and emittance measurements of solids, liquids, and gases for light with wavelengths greater than 2 μm.

However, some of the same optical design elements that are responsible for the superior performance also lead to more complicated and, in some cases, more severe sources of radiometric error in FT-IR spectra compared with their dispersive counterparts. Extensive theoretical and experimental literature exists on the subjects of detector nonlinearity,[2] interreflection effects,[3,4] ambient thermal emission,[5] and many other error sources.[6] Unfortunately, it is still not uncommon for the high signal-to-noise ratio and good measurement repeatability afforded by FT-IR spectrophotometers to be mistaken for low absolute radiometric uncertainty. While the complete radiometric characterization of even one FT-IR instrument is at present an ambitious long-term goal, it should be possible for users of FT-IR spectrometers to both understand and reduce the various sources of radiometric error through the use of standard and diagnostic samples appropriate to the measurements of interest.

As part of an effort at the National Institute of Standards and Technology (NIST) to develop a set of calibrated neutral-density filters for use as infrared transmittance standards from 2 to 25 μm, we have undertaken a program of testing and improving the radiometric accuracy of simple room-temperature FT-IR transmittance measurements of thin parallel-sided dielectric materials with or without reflective metallic coatings for nominally neutral attenuation. For the uncoated samples the expected transmittance values can be calculated in the wavelength regions where the absorption is negligible by use of the available index of refraction data. These values can be compared to the results of the FT-IR measurements. For higher attenuation values, comparisons of FT-IR and laser measurements at 3.39 μm and 10.6 μm are made for metallic coatings on ultrathin (100 nm) dielectric substrates. The ultrathin samples we have examined had Lexan substrates with a clear aperture of 15-mm diameter and were produced by Luxel Corporation of Friday Harbor, Washington. These samples are discussed further in Subsection 2.C.

The authors are with the National Institute of Standards and Technology, Optical Technology Division, Gaithersburg, Maryland 20899-0001.

Received 31 March 1997; revised manuscript received 23 June 1997.

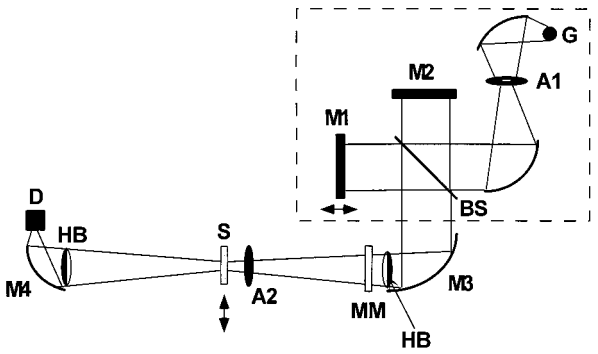

Fig. 1. Schematic optical layout for the FT-IR transmittance measurements: G, globar source; A1, source aperture; BS, beam splitter; M1, moving mirror; M2, fixed mirror; M3, off-axis paraboloidal mirror; HB, half-beam block; MM, metal mesh filter; A2, field stop; S, sample; M4, off-axis ellipsoidal mirror; D, DTGS pyroelectric detector. The transmittance is measured by our switching the sample in and out of the beam and comparing to either an empty path or a reference sample. The half-blocks, metal mesh, and field stop are used to reduce the systematic errors that are due to interreflections, detector nonequivalence, and source aperture radiation, as described in the text.

2. FT-IR Measurements

A. Experimental Setup

Transmittance measurements over the wavelength range from 2 to 25 μm at near-normal incidence were performed with a Bio-Rad FTS-60A scanning FT-IR spectrometer, by use of a ceramic globar source, Ge-coated KBr beam splitter, and a blackened deuterated triglycine sulfide (DTGS) pyroelectric detector with a KBr window. The interferograms were transformed with a zero-filling factor of 2, with boxcar apodization, and the nominal spectral resolution was 8 cm^{-1}.

The sample was placed at the focus (3-mm, 6-mm, or 8-mm spot diameter, selectable by means of a source aperture wheel) of the $f/3$ beam in the instrument sample compartment, which was purged with dry, CO_2-free air. Two samples at a time were held in a movable sample holder that allowed them to be switched vertically in and out of the beam and also provided for rotation with 1′ angular resolution and vertical translation with 5-μm resolution to test for interreflection, beam displacement, and nonuniformity effects as described below. Measurement of the background spectrum was performed before and after each sample measurement, and data were accepted only if the wavelength-averaged signal drift level was less than 0.1% relative change in transmittance over this time interval, which varied from 5 to 60 min depending on the attenuation level of the sample under test.

A schematic of the optical layout of the FT-IR measurements is shown in Fig. 1. The important optical components are labeled and defined in the caption. The half-blocks, attenuators, and field stop are used to test for and reduce several of the major radiometric error sources that are discussed below.

B. Reduction of Major Radiometric Error Sources

1. Errors Due to Interreflections Involving the Sample

Errors in the transmittance spectra can be produced by reflections between the sample and other components in the optical train, chiefly the interferometer and detector. Tests were performed to look for the effects of these interreflections on the measured transmittance spectra. This was done by measuring the ratio of the transmittance of a 0.25 mm thick Si wafer at near-normal incidence to the transmittance at 10° incidence.

The $f/3$ beam of the spectrometer was measured by rotation of a wire grid polarizer at the sample position to have roughly 7% ± 4% vertical polarization (defined in terms of Stokes parameters[7] as s_1). For this degree of polarization, and taking into account the conical beam geometry, the angle of incidence dependence of the transmittance is expected from the Fresnel equations applied to the Si sample to be less than 0.2% between 0° and 10°. Tilting the sample also increases the average optical path length for the transmitted radiation; for the largest absorption feature in the Si sample ($a \sim 20\%$ deep absorption line near 16 μm) the expected change in transmittance between 0° and 10° is 0.02%. Thus any changes larger than 0.2% in the detected flux on tilting the sample should be ascribed to an error source involving the sample, such as interreflection or beam displacement on the detector.

The results of these measurements are shown in Fig. 2(a). Curves A, B, C, and D each represent a ratio of two measurements of a Si sample, one with 0° incidence ratioed to one with 10° incidence. For the $f/3$ beam geometry at the sample, a 10° tilt is sufficient to prevent the beam reflected from the sample from re-entering the interferometer. Curve A was obtained with no additional effort to eliminate the interreflection effects in the normal incidence spectrum. The denominator should represent the transmittance of Si without interreflection from the interferometer, and the relative increase of as much as 4% in measured transmittance at normal incidence can be attributed to the combined effects of sample-interferometer and sample-detector interreflections.

Curve A has a complicated wavelength dependence, qualitatively similar to that observed by previous researchers[4] in the ratio of the apparent transmittances of reflecting and absorbing half-beam blocks placed in the sample position. There is a minimum near the center of the measured spectral range, and prominent structure near 8 μm and 3 μm. The sample-interferometer interreflection should produce contributions of alternating positive and negative signs, respectively, to the apparent transmittance for odd and even multiples of a given frequency component of the spectrum.[3] This behavior is qualitatively borne out in the data, which shows considerable structure of both signs, especially for

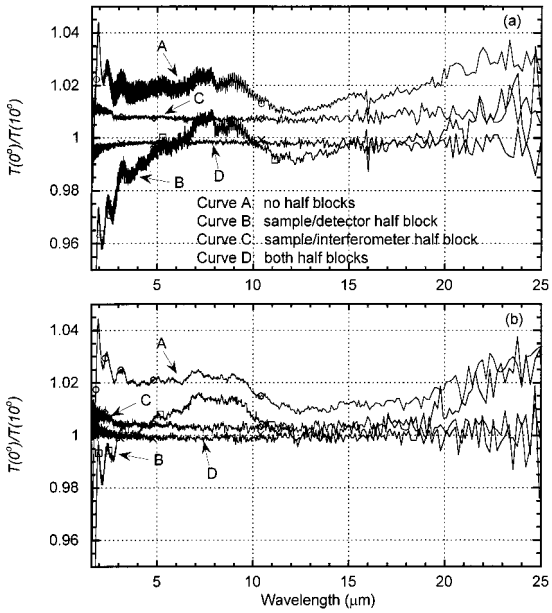

Fig. 2. Effects of sample–interferometer and sample–detector interreflections on the apparent transmittance of (a) a 0.25-mm-thick Si wafer and (b) a 27-nm-thick NiCr film on a 120-nm-thick Lexan substrate, tested by ratioing of the measured transmittance at normal incidence to that at 10° incidence. Curve A, transmittance ratio versus wavelength with no beam blocks; curve B, ratio with a half-block between sample and detector; curve C, ratio with a half-block between the sample and interferometer; curve D, ratio with both half-blocks in place.

wavelengths shorter than 15 μm, half of the cutoff wavelength of the KBr:Ge beam splitter.

For wavelengths shorter than 12 μm, there are apparent Fabry–Perot fringes in the transmittance with an amplitude as high as 0.5% and a spacing of 12.6 cm^{-1}, twice the actual spacing of 6.3 cm^{-1} observed in higher-resolution spectra (not shown in Fig. 2) of the 0.25-mm-thick Si sample. The double-spaced fringes are expected from the first-order sample-interferometer interreflection: each minimum or maximum in the true spectrum shows up again at twice the frequency, so a fringe extending from ν to $\nu + \Delta\nu$ will produce an artifact extending from 2ν to $2\nu + 2\Delta\nu$. Higher-order effects are in principle expected as well[3] but in this measurement are too weak to be discerned.

For curve B, a half-circular beam block made of infrared absorbing black felt was placed near the ellipsoidal focusing mirror for the detector (M4 in Fig. 1) in such a way as to prevent light reflected from the detector from reentering the system, and the tilting test was repeated. The sample-detector and interferometer-detector interreflections should be effectively blocked. The resulting curve for this configuration has a structure similar to curve A, but the change in apparent transmittance between 0° and 10° is smaller, at least for wavelengths greater than 5 μm.

Curve C was obtained by removal of the sample-detector half-beam block with one instead placed near the focusing paraboloidal mirror at the entrance of the sample compartment (M3 in Fig. 1). Thus the sample-interferometer and detector-interferometer interreflections should be substantially reduced,[4] but the sample-detector interreflection remains. In this case an almost wavelength-independent increase of ~1% is seen at normal incidence, of the order of the expected additive contribution of reflections between the ~50% reflecting Si sample and ~8% reflecting KBr detector window.

Finally, curve D, the results of the tilting test with both beam blocks in place are shown. In this case the average change in transmittance is less than 0.5% over the entire wavelength range (2 to 25 μm) that was measured. The remaining difference below 1.0 in the ratio $T(0°)/T(10°)$ is believed to result from beam displacement on the detector from the tilted sample.

To confirm the above analysis, we also performed the tilting tests with a 27-nm-thick NiCr film on a 120-nm-thick Lexan substrate. The results of these tests are shown in Fig. 2(b). They are qualitatively similar to those for the 0.25-mm-thick Si sample shown in Fig. 2(a). The differences can be attributed to the characteristics of the thin coated Lexan sample: the lack of Fabry–Perot fringes in curves A and B (see Subsection 2.C); the lower value in curve C consistent with the lower reflectance of the NiCr–Lexan sample for light incident from the substrate side, which was facing the detector during these measurements; and, last, the smaller residual in curve D, consistent with the negligible beam displacement for such a thin sample.

Use of the half-beam block between the sample and the interferometer is only one way of eliminating interreflections between them. It represents a compromise among (a) minimizing the range of angles on the sample, (b) minimizing the central or average angle on the sample, (c) maximizing the flux throughput to the detector, and (d) minimizing the number and extent of alterations to the standard geometry of the instrument.

The $f/3$ geometry of the Bio-Rad FTS-60A produces a conical beam focused at the sample position with the central ray at normal incidence and the edge ray at approximately 9.5° from the normal. However, the central section of the beam, from 0° to approximately 2°, is blocked inside the interferometer for use by a He–Ne laser beam for alignment and scanning. Thus, the flux-weighted average incident angle in the standard configuration is approximately 6°, with a range of angles from 2° to 9.5°. This geometry is nominally radially symmetric.

In this geometry interreflections between the sample and interferometer can be eliminated in several ways:

(1) The sample can be tilted by at least 10°. The advantages of this method are that (a) the only alteration to the normal configuration is the sample tilt and (b) there is no throughput loss. The disadvantages are (a) a loss of conical symmetry in the incident

geometry and that (b) the maximum incident angle is increased to ~20°, with the weighted average angle increased to ~12°.

(2) A second method (which was used here) is to place a half-beam block near the input focusing mirror. The advantage is that the standard range of incidence angles and sample orientation are maintained. The disadvantages are (a) a reduction in throughput by a factor of 2, (b) loss of radial symmetry (although the conical symmetry is retained in the remaining quadrants), and (c) increased sensitivity to beam wander, as the presence of a knife-edge in the beam can effectively amplify changes in signal level resulting from the beam moving on the detector.

(3) Nearly equivalent to the second method would be a combination of aperturing the beam at the focusing mirror to reduce the cone half-angle from 9.5° to 5° and then tilting the sample by 5°. The disadvantages of this method are a significant loss of throughput due to the empty region of the beam from 0° to 2° and the loss in conical symmetry.

(4) A fourth alternative would be to replace the sample compartment optics and hardware to provide an $f/6$ geometry with the central ray at 5° incidence on the sample. This approach would combine the advantages of the other methods while eliminating their disadvantages (except for the loss of conical symmetry). The disadvantages are (a) the reconstruction or external setup of a new sample compartment and optics and (b) a doubling of the focused spot diameter on the sample (owing to conservation of throughput). Reconstruction would entail replacing the focusing mirrors between the sample and interferometer and between the sample and detector, as well as doubling the path length between the focusing mirrors.

(5) Finally, interreflections can be reduced by placing an attenuator such as a neutral-density filter between the sample and interferometer. The attenuator must itself be tilted by at least 10° to avoid introducing additional interreflection effects and also must be sufficiently large to avoid beam vignetting. For a 10% transmitting attenuator, the sample-interferometer interreflection error should be reduced by a factor of 100. The disadvantages are (a) a major reduction in throughput (a factor of 10 in this example) and (b) alignment changes due to beam deviation or deflection.

For this study the second approach was selected. It is a relatively simple one to implement and does not increase the weighted average angle of incidence or destroy the normal-incidence conical symmetry; thus it does not increase the errors due to angle-dependent effects. Also, as described below, it allows the positioning of a second block after the sample without additional throughput loss. For future research a variation of the third approach is being implemented, which will allow a variation of beam geometry from $f/3$ to nearly collimated.

Interreflection between the sample and the detector takes place in a different geometry. On the input side the sample has light focused onto it by an off-axis paraboloidal or spherical mirror from an input collimated beam. On the output side of the sample, the diverging beam is refocused onto a detector by an off-axis ellipsoidal mirror. The sample center and the detector are generally placed at the two foci of the ellipsoid. This easily leads to multiple interreflections between the sample and detector.

Again, one way to eliminate this problem is (1) to tilt the sample, which has the same advantages and disadvantages as mentioned above. Also, (2) the detector may be tilted. But because the detector collection optics geometry is generally very fast, $f/1$ or even $f/0.5$, the tilt angle required, 30° or 60°, becomes difficult to implement. (3) A third alternative is to use only low reflectance detectors, such as a windowless black-coated detector, or to use a detector with an integrating sphere as a collector. Black-coated windowless detectors are not available for all wavelengths of interest. Use of an integrating sphere significantly reduces the system throughput and requires reconstruction of the hardware. (4) Placement of an intervening attenuator similar to one discussed above will also reduce interreflections but will have similar disadvantages. Finally, (5) an additional half-beam block can be used to prevent light reflected off the detector from reaching the sample.

Method (5) was used here. When combined with the input half-beam block and placed appropriately, the second beam block does not further reduce the throughput to the detector. The disadvantage is an increased sensitivity to beam wander owing to the sample's interaction with the beam (beam deflection and beam deviation). In practice the first beam block is positioned to block slightly more than half of the beam, and the second beam block slightly less, to reduce the sensitivity to sample-induced beam displacement on the detector. Finally, we note that the second half-beam block adopted in this work has the additional advantage of eliminating interreflections between the detector and interferometer, which are present with or without the sample in place and can affect both the reference and sample measurements.

2. *Errors Due to Source Aperture Heating*

Ideally, an image of a portion of the source, defined by the Jacquinot stop in the source compartment of the FT-IR spectrophotometer (A1 in Fig. 1), is transferred to the sample and detector by the optics of the instrument. This is at least approximately the case, as can be observed by examining the visible portion of the beam passing through the instrument. However, the source aperture is heated by the source radiation and itself becomes a source of near-ambient blackbody radiation with a large effective area. Thermal emission from components of the system other than the source is known to produce substantial errors in FT-IR spectra[5] when either the sample or detector temperature is far from ambient. In the present case, where both the sample and detector are near room temperature, the radiation from the slightly

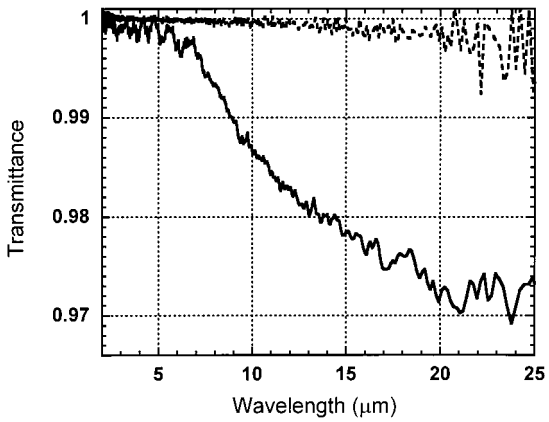

Fig. 3. Transmittance of a 15-mm diameter aperture with a nominal beam diameter of 3 mm at the sample position. The solid curve shows the measured transmittance without field stop A2 (Fig. 1), and the dashed curve shows the results with A2. The reduced transmittance observed at longer wavelengths without A2 is attributed to overfilling of the aperture as a result of thermal radiation from the heated source aperture.

heated source aperture can still overfill the sample area, producing spurious transmittance results.

This effect is demonstrated in Fig. 3, in which measurements of a 15-mm aperture placed at the sample position with a nominal spot diameter of 3 mm are shown. The solid curve shows the measured transmittance, which is close to 1.0 for wavelengths less than 7 μm, but falls off sharply toward longer wavelengths, reaching a value near 0.97 by 25 μm. This behavior is consistent with a wavelength-dependent effective spot size, which overfills the 15-mm aperture at longer wavelengths, where the blackbody radiation from the heated source aperture is a larger fraction of the ~1200-K blackbody spectrum of the globar source. To try to reduce this effect, we placed a second aperture (A2 in Fig. 1) in front of the sample and reduced its size to slightly clip the beam, making it effectively the field stop for the system. This aperture was also tilted by ~45° to avoid additional interreflections. The transmittance of the 15-mm aperture with A2 in place is shown as the dashed curve in Fig. 3. The falloff in transmittance at longer wavelengths is now less than 0.2%.

The use of secondary aperture A2 was adopted for the remaining transmittance experiments described in this paper. Because A2 is not in the image plane, it produces some degree of vignetting, which is also the case with the half-blocks described earlier. This vignetting should be expected to increase the sensitivity of the transmittance measurement to sample nonuniformity. It would be preferable to place the secondary aperture A2 at a focal position, which would be possible with additional focusing mirrors in the beam path. Another possible solution would be to preaperture the source before the Jacquinot stop in the source compartment, thus reducing the temperature rise of this aperture. Finally, nonsource emission effects can be largely removed by chopping the source directly,[5] either using a double-modulation scheme with the rapid-scan FT-IR design, or the more conventional step-scan approach. Of course, chopping the source decreases the throughput by a factor of two.

3. *Errors Due to Detector Nonequivalence*

Another class of important error sources in FT-IR transmittance measurements is detector nonlinearity–nonequivalence effects.[8] In the case of the pyroelectric DTGS detector used in this study, the nonlinearity is a small effect, which can be seen in the signal below the cutoff of the KBr:Ge beam splitter, typically $<10^{-4}$ of the peak single-beam signal. However, the responsivity of DTGS detectors is temperature-dependent near room temperature, so that the change in radiant flux on the detector as the sample is switched in and out of the beam can produce a nonequivalent response and shift the apparent transmittance accordingly.

To test for this effect, we measured the transmittance of the 0.25-mm-thick Si wafer versus the empty beam with increasing amounts of beam attenuation achieved by our placing one or two metal mesh screens before the sample and closing down the field stop A2 (see Fig. 1). Closing down this stop also reduces somewhat the solid angle of the beam, since the stop is not at a focal plane; however, for the nearly unpolarized beam this effect is estimated to produce a relative change of less than 0.05% in measured transmittance. The results of this test are shown in Fig. 4. The measured transmittance of the Si wafer from 2 to 5 μm is shown in Fig. 4(a) for varying degrees of attenuation, denoted by the detector signal at zero path difference (ZPD) with the sample removed from the beam. Apparent in this figure is a nearly wavelength-independent relative increase of 2% in the measured transmittance value as the power level is decreased.

When the incident flux level is decreased by ~1 order of magnitude from the unattenuated beam (which contains only half of the original flux of ~25 mW because of the presence of the half-blocks), the measured transmittance approaches the solid curve. This curve shows the transmissivity calculated for normal incidence, including incoherent addition of multiple reflections, from handbook values[9] of the index of refraction, n, according to the following formula:

$$T = \frac{1 - r}{1 + r}, \tag{1}$$

where $r = (1 - n)^2/(1 + n)^2$ is the single-surface power reflection coefficient. The imaginary part of the index is negligible ($<10^{-7}$) in this spectral range. The spread in the published values for n in the 2- to 5-μm range obtained by two different techniques (minimum deviation in a wedge[10] or observation of channel spectra in an optical flat[11]) is ~0.2%.

In Fig. 4(b) the measured transmittance values at 3.4 μm seem to saturate to an average level within 0.2% of the expected value for ZPD levels of less than

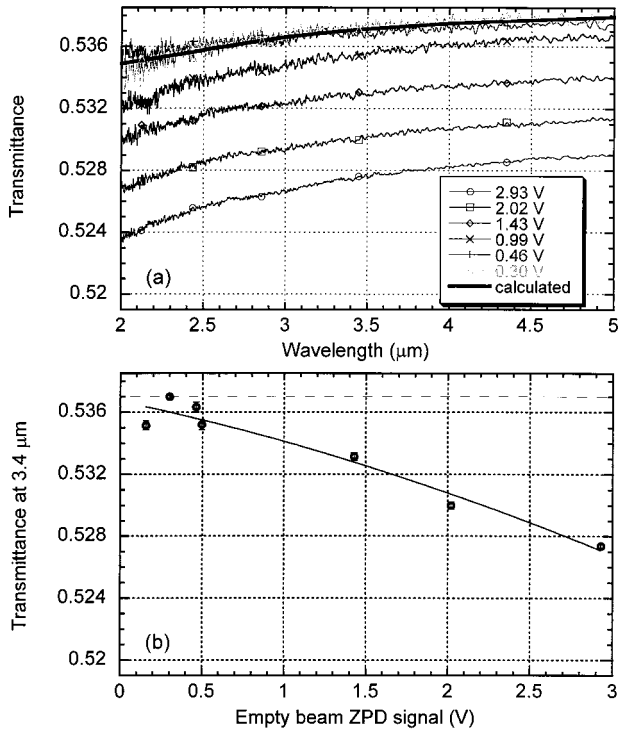

Fig. 4. Measured transmittance of a 0.25-mm-thick Si wafer versus wavelength for different incident power levels. (a) Measured transmittance curves from 2 to 5 μm for different values of the empty beam detector signal at ZPD, compared with the predicted transmittance based on handbook values for the index of refraction. (b) Dependence of the apparent transmittance at 3.4 μm on ZPD signal (open circles, data; solid line, quadratic fit). The measured transmittance approaches the expected value as the incident power level is decreased, reducing the temperature change of the detector.

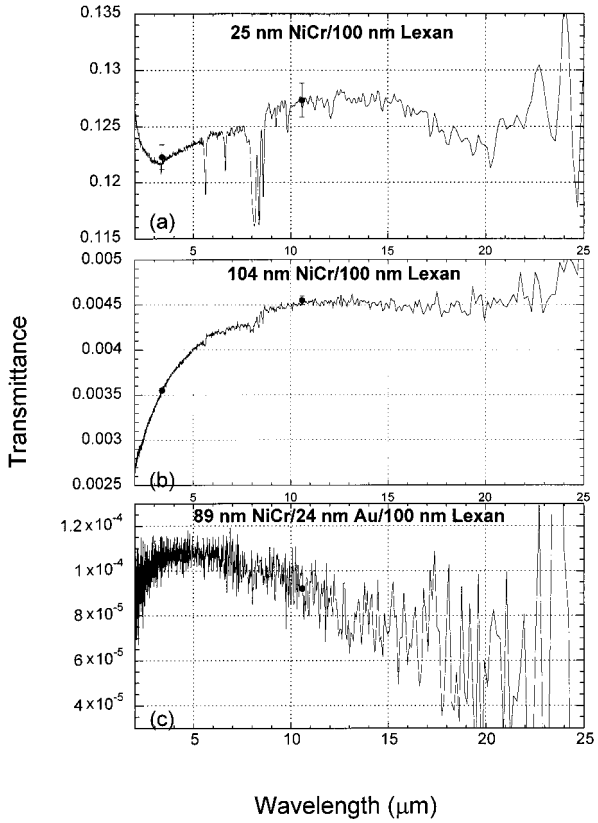

Fig. 5. Comparison of FT-IR and laser transmittance measurements of three metallic thin-film neutral-density filters on 100-nm Lexan substrates: (a) 25-nm NiCr, (b) 104-nm NiCr, and (c) 89-nm NiCr/24-nm Au coatings. Curves, FT-IR data; filled circles, laser data at 3.39 μm and 10.6 μm with expanded uncertainty error bars as described in the text. The laser and FT-IR data appear to agree within the expanded uncertainties.

0.5 V. The scatter (~0.4%) in the four data points at the lowest power levels is reproducible (not the result of random drifts in the interferometer—the error bars show the statistical uncertainty components), but the origin of the differences is not well understood. They are likely related to the small amount of flux scattered by the metal mesh screens or field stop A2 that reaches the detector. In any case the radiometric accuracy of the transmittance measurement is demonstrably improved by attenuating of the beam as we have done here. Transmittance measurements of samples relative to the empty beam were thus performed with empty beam ZPD levels of <0.5 V for the laser intercomparison measurements described in the Subsection 2.C. This represents a large decrease in the signal-to-noise ratio for a given averaging time and thus partially negates the multiplexing advantage of the FT-IR design. Other possible approaches are discussed in Section 5.

C. Measurement of Samples for Intercomparison with Laser Sources

Comparison of broadband low-resolution transmittance spectra of thin parallel-sided dielectric samples with coherent narrow-band laser measurements is in general complicated by Fabry–Perot interference effects. In principle, sufficiently high-resolution measurements could be made with the FT-IR instrument to map out the interference fringes and compare directly with the laser result (assuming the laser wavelength is sufficiently well known). However, in practice, differences in the beam geometry between the two measurements, as well as a slight tilt, wedge, or nonflatness of the sample, make this type of comparison difficult at the 0.1% relative standard uncertainty level that one would like to achieve.

Our approach has been to use samples that are free of interference effects so that the broadband 8-cm^{-1} resolution FT-IR data can be compared easily with the laser measurements. Such samples consist of metallic NiCr or Au coatings on ~100-nm-thick Lexan substrates, which are thin enough that the entire wavelength range of interest (2–25 μm) is contained within the first interference fringe.[12] (The position of the longest wavelength transmittance minimum is given by $\lambda = 4nd \sim 4(1.5)(0.1\ \mu m) = 0.6$ μm, where d is the substrate thickness).

Results of FT-IR transmittance measurements of three metallic film samples on ~100-nm Lexan substrates are shown in Fig. 5. For the 25-nm NiCr

sample shown in Fig. 5(a), the transmittance measurement was made relative to the empty beam with the setup with reduced radiometric errors described in the previous section. This sample shows a fairly flat attenuation, with the transmittance varying between 0.12 and 0.13 over the measured spectral range. A number of absorption features from the Lexan substrate can be seen in the 5–10-μm region. The spectra of the higher-optical-density samples shown in Figs. 5(b) and 5(c) were obtained by removal of the metal mesh filters; for the 104-nm NiCr sample in Fig. 5(b) the sample with the 25-nm NiCr film was used as a reference, and for the 89-nm NiCr/24-nm Au sample in Fig. 5(c) the aperture stop A1 was opened to 8 mm, and the 104-nm NiCr sample was used as a reference. By this method the ZPD signal was kept well under 0.5 V in the reference beam for all three measurements to reduce the detector nonequivalence error.

As is apparent in Fig. 5(b), the transmittance of the 104-nm NiCr coating on Lexan has substantial wavelength dependence for wavelengths shorter than 10 μm. The signal-to-noise ratio is less than that of the laser transmittance measurement (discussed in Section 3). The 89-nm NiCr/24-nm Au sample shown in Fig. 5(c), on the other hand, has a transmittance of less than 10^{-4} at 10.6 μm, so that even with an averaging time of more than 1 h used to obtain this spectrum, the noise level is much larger than that obtained with the laser measurements. The spectral variation is slow enough, however, that a comparison of the average transmission over a 1-μm interval to the laser measurements is still of interest. Lower radiometric uncertainty can probably be achieved for this type of sample by use of a photoconductive detector.

3. Laser Measurements

Two laser sources were used to make transmittance measurements on the samples described in the previous section: a He–Ne laser at 3.39 μm and a CO_2 laser at 10.6 μm. The CO_2 laser system in the Optical Technology Division at NIST is set up to be used in either heterodyne mode or direct mode and has been described previously.[13] The He–Ne system was a direct transmittance setup, employing a beam splitter and reference detector to improve the signal stability by ratioing the signal of the two detectors. In each laser system the sample was swapped repeatedly in and out of the beam to yield statistics on the transmittance value as well as to cancel out residual drift and improve the signal-to-noise ratio.

In the 10.6-μm system the sample was placed either in one arm of the interferometer (heterodyne mode) or after the second beam splitter (direct mode), and the data from both sets of measurements were found to agree to within the statistical uncertainty. The 3.39-μm transmittance measurements were performed with a pyroelectric detector for the 25-nm and 104-nm NiCr film samples, measured relative to the empty beam, and a photovoltaic InSb detector for the 89-nm NiCr/24-nm Au film sample, which was measured relative to the 104-nm NiCr film sample. The results of the laser transmittance measurements are shown as filled circles in Fig. 5, and the error bars represent the expanded uncertainties, which are explained in Section 4.

4. Uncertainty Analysis

The following subsections list sources of ordinate scale error in the FT-IR[6] and laser transmittance measurements that we believe may be important in the present study. In each case we have either performed a test to estimate the size of the uncertainty in the measured transmittance that results from the given effect or estimated it on the basis of geometrical or other arguments. Many of the uncertainty sources are difficult to isolate from one another, and we indicate where more rigorous tests are planned. Tables 1–3 list our estimated type B (systematic) relative standard uncertainty components,[14] evaluated by various means (given relative to the measured transmittance value, unless noted), and then the relative standard uncertainty based on statistical analysis of the repeatability of the measurements, for each of the three samples that were used for intercomparison with the laser measurements.

The type B uncertainties, although in general not orthogonal, are added in quadrature because their detailed interdependencies are not well understood. Then the type A uncertainty is added in quadrature to this sum, and the final uncertainty is multiplied by 2, so that the quoted relative expanded uncertainties in Tables 1–3 represent approximate 95% confidence intervals. For the case of the 89-nm NiCr/24-nm Au sample, the uncertainty is added in quadrature to that of the 104-nm NiCr sample, which was used as the reference sample for this measurement. The final results for the transmittance values at the intercomparison wavelengths for the FT-IR and laser measurements, with the expanded uncertainties, are listed in Table 4.

A. FT-IR Measurements

The following is a discussion of the relative standard uncertainty estimates for the FT-IR transmittance values, which are summarized in Table 1.

1. 0% Transmittance Level Offset

FT-IR instruments are intrinsically ac-coupled devices, since the FT process naturally removes the unmodulated portion of the flux incident on the detector. However, it is still possible for false modulated signals to be present because of coherent electrical noise sources in the local environment or because of flaws in the amplification, digitization electronics, or software, leading to an apparent transmittance signal even when no modulated flux is reaching the detector. This possibility was tested by placing an opaque metal disk in the place of the sample. No signal was found above the noise floor of 10^{-5} transmittance for the one hour averaging time and the DTGS detector used in the current experiment. Based on other measurements

Table 1. FT-IR Transmittance Relative Standard Uncertainty Components (% Measured Value)

Uncertainty Source	25-nm NiCr/100-nm Lexan	104-nm NiCr/100-nm Lexan	89-nm NiCr/24-nm Au/100-nm Lexan
Type B			
0% offset	0.00	0.00	0.00
Interreflections	0.20	0.35	0.40
Detector nonlinearity	0.10	0.10	0.10
Detector nonequivalence	0.20	0.20	0.20
Nonsource emission	0.15	0.15	0.15
Sample nonuniformity	0.20	0.20	0.20
Beam, sample, detector nonuniformity	0.20	0.20	0.20
Beam displacement, deviation, focus shift	0.00	0.00	0.00
Beam geometry, polarization	0.15	0.15	0.15
Sample vignetting	0.03	0.03	0.03
Sample scattering, diffraction[a]	0.00	0.00	0.00
Apodization errors	0.00	0.00	0.00
Phase errors[a]	0.00	0.00	0.00
Sample temperature change[a]	0.00	0.00	0.00
Sample aging	0.30	0.00	0.00
Quadrature sum	0.55	0.55	0.58
Type A			
Relative standard uncertainty of mean at 3.39 μm	0.14	0.32	3.30
Relative standard uncertainty of mean at 10.6 μm	0.22	0.27	5.00
Relative expanded uncertainty at 3.39 μm	1.14	1.27	6.82
Relative expanded uncertainty at 10.6 μm	1.19	1.22	10.14

[a]Not tested; assumed negligible.

on this and similar FT-IR instruments with more sensitive photoconductive detectors, we believe the intrinsic offset to be less than 10^{-7} in transmittance,[15] so we choose not to include it in the uncertainty budget.

2. Interreflections

Interreflection effects are a large source of radiometric error, as was discussed in Subsection 2.B.1, where we described our efforts to minimize interreflections involving the sample. Interreflections involving

Table 2. 3.39-μm He–Ne Laser Transmittance Relative Standard Uncertainty Components (% Measured Value)

Uncertainty Source	25-nm NiCr/100-nm Lexan	104-nm NiCr/100-nm Lexan	89-nm NiCr/24-nm Au/100-nm Lexan
Type B			
0% offset	0.01	0.01	0.01
Interreflections	0.10	0.10	0.10
Detector nonlinearity	0.10	0.10	0.20
Nonsource emission	0.00	0.00	0.00
Sample nonuniformity	0.20	0.20	0.20
Beam, sample, detector nonuniformity	0.20	0.20	0.20
Beam displacement, deviation, focus shift	0.00	0.00	0.00
Beam geometry, polarization	0.03	0.03	0.03
Sample vignetting	0.01	0.01	0.01
Sample scattering, diffraction[a]	0.00	0.00	0.00
Sample temperature change[a]	0.00	0.00	0.00
Sample aging	0.30	0.00	0.00
Quadrature sum	0.44	0.32	0.36
Type A			
Relative standard uncertainty of mean	0.01	0.01	0.01
Relative expanded uncertainty	0.87	0.64	0.96

[a]Not tested; assumed negligible.

Table 3. 10.6-μm CO_2 Laser Transmittance Relative Standard Uncertainty Components (% Measured Value)

Uncertainty Source	25-nm NiCr/100-nm Lexan	104-nm NiCr/100-nm Lexan	89-nm NiCr/24-nm Au/100-nm Lexan
Type B			
0% offset	0.00	0.00	0.00
Interreflections	0.00	0.00	0.00
Detector nonlinearity	0.03	0.03	0.03
Nonsource emission	0.00	0.00	0.00
Sample nonuniformity	0.20	0.20	0.20
Beam, sample, detector nonuniformity	0.20	0.20	0.20
Beam displacement, deviation, focus shift	0.00	0.00	0.00
Beam geometry, polarization	0.03	0.03	0.03
Sample vignetting	0.01	0.01	0.01
Sample scattering, diffraction[a]	0.00	0.00	0.00
Sample temperature change[a]	0.00	0.00	0.00
Sample aging	0.30	0.00	0.00
Quadrature sum	0.41	0.29	0.29
Type A			
Relative standard uncertainty of mean	0.40	0.45	0.47
Relative expanded uncertainty	1.15	1.07	1.10

[a]Not tested; assumed negligible.

multiple passes through the interferometer result in false signals of alternating sign at harmonics of the actual (physical) wave number of a particular spectral component.[3,4] Other interreflections, if they involve the sample, merely add to the apparent transmittance of the sample. Errors as great as 10% were noted for reflective neutral-density filter samples without the beam blocks, but with the beam blocks the change in apparent transmittance of a NiCr/Lexan sample was less than 0.2%. Other interreflections involving the interferometer but not the sample, such as reflections between the interferometer and source aperture, also can lead to spurious spectral components, which we have not tested for. We assign a value from 0.2% to 0.4% to the relative standard uncertainty that is due to interreflections for the metallic film samples (because of the varying reflectance levels).

3. *Nonlinearity in Detector/Electronics*

Distortion of the transmittance spectrum owing to nonlinearity is most apparent in spurious signals at wave numbers below which the beam splitter is opaque. In the present case, with the signal always attenuated by at least a factor of 20, the below-cutoff signal was never observed to be larger than 1×10^{-4} of the peak single-beam signal. Also, as shown in Fig. 4, the shape of the Si transmittance spectrum between 2 and 5 μm is nearly unaffected by the changes in flux on the detector of at least a factor of 10. Measurements of narrow-band filters under similar conditions revealed some nonlinearity error (showing up as false transmittance at twice the main band wave number) at the 0.1% level. We assign a value of 0.1% to the relative standard uncertainty in transmittance that is due to detector nonlinearity.

4. *Nonequivalence in Detector Response*

A large nonequivalence effect of as great as 3% in relative transmittance level was observed when the unattenuated beam was used as a reference for sample measurement. Reducing the incident flux by a factor of 20 was found to yield transmittance values for Si from 2 to 5 μm that vary by less than 0.3% from the expected values. Based on the apparent slope in the transmittance level at 3.4 μm versus ZPD voltage level shown in Fig. 4(b), we estimate the relative standard uncertainty component that is due to residual nonequivalence error to be 0.2%.

Table 4. Comparison of the FT-IR and Laser Transmittance Values for the Three Samples Discussed in the Text[a]

Sample	3.39-μm FT-IR	3.39-μm Laser	10.6-μm FT-IR	10.6-μm Laser
25-nm NiCr	0.1217 ± 0.0014	0.1223 ± 0.0011	0.1272 ± 0.0015	0.1274 ± 0.0015
104-nm NiCr	$0.00354 \pm 4.5 \times 10^{-5}$	$0.003551 \pm 2.2 \times 10^{-5}$	$0.00452 \pm 5.5 \times 10^{-5}$	$0.00455 \pm 4.8 \times 10^{-5}$
89-nm NiCr/24-nm Au	$1.05 \times 10^{-5} \pm 7.2 \times 10^{-6}$	$1.06 \times 10^{-4} \pm 1.0 \times 10^{-6}$	$9.8 \times 10^{-5} \pm 9.9 \times 10^{-6}$	$9.2 \times 10^{-5} \pm 1.0 \times 10^{-6}$

[a]The expanded uncertainties in transmittance derived from the values in Tables 1–3 are also listed.

5. Nonsource Emission Errors

Errors due to source-aperture emission's overfilling the sample were substantially reduced on the placement of field stop A2 (Fig. 1) before the sample. Figure 3 shows that there may be a 0.1%–0.2% residual effect for wavelengths greater than 10 μm even with A2 in place. Emission from the sample or detector[5] is not expected to cause significant error because both are near room temperature. A test was performed with the source blocked, and no interferogram was detected above the $\sim 10^{-5}$ noise level. We estimate the relative standard uncertainty that is due to nonsource emission errors to be 0.15%.

6. Sample Nonuniformity

The uniformity of the Lexan neutral-density filter samples was tested with a 3-mm diameter spot moved on the sample by 3 mm in two orthogonal directions perpendicular to the sample normal. The maximum spatial variation was found to be 0.4% in the 9-mm-diameter circle centered at the center of the film. In principle this need not be a source of error if the sample is mapped completely and the beam and detector uniformities are known as well (see Subsection 4.A.7). The transmittance can then be defined as the appropriate spatial average. However, the absolute position of the sample relative to the beam was known only to within 1 mm. Since the transmittance measurements to compare with the lasers were performed with a 6-mm aperture, and the laser measurements had different spot sizes, we assign a relative standard uncertainty of 0.2% to sample nonuniformity for the metal film/Lexan samples.

7. Interaction of Sample, Beam, and Detector Nonuniformity

Even if the position of the spot on the sample is well defined and the uniformity map of the sample is known, nonuniformity in the beam and detector can produce errors in the transmittance spectrum owing to nonuniform averaging over the sample area. This effect was tested for by our flipping the sample by 180° without moving it relative to the beam; the estimated relative standard uncertainty is 0.2% for the Lexan samples.

8. Beam Displacement, Deviation, or Focus Shifting

Error introduced by beam displacement, deviation, or focus shifting is negligibly small for the thin metal-coated Lexan samples. Tests are planned of the general size of these effects for different types of sample by measurement of the transmittance of variable thickness and variable wedge-angle Si wafers.

9. Beam Geometry, Polarization Effects

Because the beam geometry and polarization states are different for the laser and the FT-IR measurements, the measured transmittance values would not in general agree even in the absence of other sources of error. The laser geometry is nearly collimated, normal incidence, and highly polarized. In contrast, the half-angle of the beam in the sample compartment of the Bio-Rad FTS-60A spectrophotometer is nominally 9.5°, and the central portion (~2°) of the beam is blocked for use by the alignment He–Ne laser. With the half-beam blocks in place, the geometry at the sample position is a half cone with an average angle of incidence of 6°, but with the axis of the cone aligned perpendicular to the sample to within 0.5°. Because of the conical geometry, the polarization of the beam is unimportant as long as the cone is normal to the sample surface,[16] and the transmittance is calculated to be of the order of 0.05%–0.2% lower than the collimated normal incidence value. The difference is wavelength and thickness dependent, being greatest for the shortest wavelengths and thickest samples.

In principle, one could account for the deviation from normal-incidence, collimated incident radiation in the FT-IR measurement when comparing with the laser measurements. However, there is sufficient uncertainty in the actual flux distribution of the FT-IR beam that we include the differences between the two geometries as part of the uncertainty in the measured transmittance.

10. Sample Vignetting

We tested vignetting by placing a blank aperture of the same size as the sample in the beam and measuring its transmittance. Other than the possible residual effects from the source aperture radiation for wavelengths longer than 6 μm already discussed (Subsection 4.A.4), no effects of sample vignetting have been observed, and the relative standard uncertainty is estimated to be less than 0.03%.

11. Scattering or Diffraction by the Sample

Scattering or diffraction by the sample can cause the measured transmittance of the sample to depend on the geometry of the collection optics of the detector system. It can in principle be tested by placing a series of baffles after the sample and looking for any change in the detector signal. This test has not been performed. Backscattering into the beam by the baffles could complicate this analysis. Another possible test is to measure the transmittance with an integrating sphere. At this time we estimate this error source to be negligible.

12. Apodization Effects

The interferograms for the background and sample spectra were transformed with either boxcar or triangular apodization, and no differences were noted in the spectra to within the minimum noise level. Self-apodization due to the finite source size and imperfections in the optical components of the interferometer may degrade the resolution from the nominal 8 cm^{-1} value and result in wave-number errors of at most 0.2 cm^{-1} for the largest (8 mm) spot diameter. Since the spectra are not strongly wavelength dependent near the laser intercomparison

points, this error source is not expected to be important in our analysis.

13. Interferometer Phase Errors/Phase Drift

Improper phase correction of the interferogram can cause a number of errors, including a false slope of the transmittance curves. This effect was not tested directly but is folded into the repeatability estimate given below. Wavelength errors due to drift in the FT-IR He–Ne laser wavelength are estimated to be less than 0.05 cm^{-1} and are considered unimportant for these samples, which are free from spectral structure at the points where the laser–FT-IR intercomparisons are made.

14. Sample Temperature Change or Drift

Sample temperature effects were also not tested for directly; we plan to measure the temperature dependence of the samples near room temperature to provide an estimate for this error source. This source of error is not expected to be significant for the metal films, whose electronic relaxation rates are dominated by impurity scattering, which is fairly independent of temperature.

15. Sample Aging

All the samples were measured more than once over a 10-month period, and no observable time dependence was found except for the 25-μm NiCr/100-nm Lexan sample, which may have oxidized somewhat over time and become more transparent by as much as 2%. However, the last measurements of this sample were performed both with the laser and the FT-IR systems within 2 months of each other, and changes observed over this amount of time were no more than 0.3%. We take this as the relative standard uncertainty for this sample.

16. Type A Uncertainty (Random Noise/Drift/Repeatability)

All the spectra shown in Fig. 5 exhibit apparently random fluctuations from one data point to another, which are believed to result from noise in the DTGS detector. In addition, drifts in the temperature or position of optical components in the FT-IR spectrophotometer, or in the atmosphere inside the instrument, can cause shifts in the spectra on a time scale longer than that of an individual scan. Both of these effects can be reduced by averaging of spectra taken at different times. The uncertainties from these random effects were estimated by performance of several successive measurement runs with the interferometer and evaluation of the standard deviations at each wave number. For comparison with the laser measurements, the transmittance was averaged over a 16-cm^{-1} interval. The values of the relative standard uncertainty taken as the standard deviation of the mean are listed in Table 1.

B. Laser Measurements

Below is a description of uncertainty sources for the laser measurements. These estimates are summarized in Table 2 (3.39 μm) and Table 3 (10.6 μm).

1. 0% Transmittance Level Offset

The 0% transmittance level effect was measured by our blocking the laser beam; and where need be, it was subtracted from both sample and reference measurements. It was found to be significant only in the case of the 3.39-μm laser measurement, where there was a slight zero offset in the lock-in amplifier. In the 10.6-μm measurement the offset was below the noise floor of the detector–amplifier system.

2. Interreflections

The effect of interreflections was tested by our rotating the sample about an axis perpendicular to the beam for both *s* and *p* polarized light and checking to see how well the angle-of-incidence dependence followed the expected behavior from the Fresnel equations. The transmittance was found to follow the expected curves with no evidence of a central bump in the transmittance versus angle curve at the level of 0.1% relative to the transmittance at normal incidence. The relative standard uncertainty that is due to this error source is estimated to be less than 0.1%. Backreflections from the sample into the laser can affect the laser output, but this effect was not observed in the reference detector measurement with the 3.39-μm system or in the 10.6-μm system, where statistically indistinguishable values for transmittance were obtained with either the heterodyne or direct method.

3. Nonlinearity in Detector or Electronics

The power level dependence of the transmittance values were tested, and the beam was attenuated to the point at which the transmittance changed by less than 0.1% versus power level. In the case of the 3.39-μm system a power level of less than 1 mW was used with a pyroelectric detector, and less than 10 μW with a photovoltaic detector. In the 10.6-μm system the power level was approximately 5 mW. The electronics were calibrated against known standards. The relative standard uncertainty that is due to the combined effects of these errors is estimated at 0.1%.

4. Nonsource Emission

In the 3.39-μm system, unwanted light from the laser was filtered out to at least the 10^{-5} level. The laser beam was chopped to reduce stray light effects. Blocking the beam with an opaque object always yielded just the noise floor of the electronics and detector. In the 10.6-μm system the modulation of the two beams at a relative difference frequency of 30 MHz is extremely effective at eliminating background (thermal) radiation.[13] This error source is considered unimportant on the scale of this intercomparison test.

5. Sample Nonuniformity

We tested the uniformity of the samples by moving the samples relative to the incident beam to several different positions and estimating a standard deviation in the resulting transmittance values. In each case the spot diameter at the sample position was approximately 5 mm. The variation was found to be of the order of 0.2% as in the FT-IR measurements, and we take this value for the relative standard uncertainty.

6. Beam Displacement, Deviation, or Focus Shifting

For these ultrathin samples, the effect on the beam geometry of the sample is negligible for beam displacement, deviation, or focus shifting.

7. Beam Geometry or Polarization

The beam geometry for the laser measurements was at least $f/80$ or even more collimated. In both systems the beam was highly polarized. Rotating the polarization with the beam at normal incidence on the sample did not produce any effect above the 0.1% level on the measured transmittance. Residual strains in the Lexan substrate could have produced some change in the transmitted polarization state through the sample, possibly affecting the measured transmittance because of the polarization sensitivity of the detector; however, this effect was not observed. The angle of incidence was less than 0.5°, at which angle the transmittance could be different from the normal-incidence value by 0.03%. This is our estimate for the relative standard uncertainty of the measured transmittance from the ideal normal-incidence value for the laser measurements that is due to beam geometry and polarization effects.

8. Sample Vignetting

The beam diameter at the sample position in each of the laser measurements was approximately ⅓ of the sample diameter. In each case the sample was replaced by an empty ring with the same clear aperture, which was found to have a transmittance of 1 within the statistical significance of the measurements. Thus vignetting is considered to be negligible as an error source for these measurements.

9. Scattering or Diffraction by Sample

Sample diffraction or scattering was not tested for directly but for the given wavelengths and spot diameters is not expected to produce significant errors in the measurements.

10. Type A (Statistical) Uncertainty

The samples were repeatedly moved in and out of the beam to permit us to collect statistics and correct for drift in the lasers and detectors. The mean value and the standard deviation of the mean were calculated, and the components of relative standard uncertainty are shown in Tables 2 and 3.

5. Conclusions

We have made FT-IR and laser transmittance measurements of several thin-film samples with optical densities in the range from 1 to 4 and found at best 0.5% relative differences between the two types of measurement. We obtained these results by reducing as much as possible the known sources of radiometric error in the FT-IR system, with the largest errors found to come from interreflection and detector nonequivalence effects. In all cases the laser and FT-IR measurements agree to within the estimated expanded uncertainty levels, although for the highest-optical-density metallic film sample the comparison is less meaningful because of the noise in the FT-IR measurement.

Commonly available optical detectors for this spectral range exhibit poor linearity. Our approach has been to attenuate the beam to the point at which the response becomes linear, thus trading dynamic range for improved linearity (and losing much of the multiplexing FT advantage). This limits the major benefit of the present comparison, with the DTGS detector, to measurements of samples with optical densities less than 2.5. Clearly a better approach would be to use a more sensitive photoconductive detector and directly measure its response curve by comparison, ultimately, to the NIST High Accuracy Cryogenic Radiometer. Preliminary results obtained by comparison of HgCdTe photoconductor and Si bolometer detectors at 1.32 μm to a Ge photoconductor calibrated against the High Accuracy Cryogenic Radiometer have shown that the effects of the nonlinear and nonequivalent detector response can be largely removed,[17] at least over part of the spectral range of each detector. These comparisons can be made at only a few laser lines, so broad absolute calibration remains difficult to perform at the high-optical-power levels (~50 mW) typical of FT-IR instruments.

In addition, intercomparison tests are planned with dispersive instruments, as well as with additional laser wavelengths including 5.3 μm and with diode lasers for wavelengths greater than 11 μm. Further work on differentiating the various error sources is planned by methodical study of samples of varying thickness, wedge angle, and reflectance. With the use of more sensitive, calibrated detectors, it is expected that the radiometric accuracy can be significantly improved, especially for higher-optical-density samples.

We thank Alan Migdall and Alan Pine for help with the laser transmittance measurements at 10.6 μm and 3.39 μm, respectively. Also, we thank Claude Roy of Bomem, Inc., for suggesting the circular half-beam block method of reducing interreflection errors.

References

1. P. R. Griffiths and J. A. de Haseth, *Fourier Transform Infrared Spectroscopy* (Wiley-Interscience, New York, 1986); D. R. Mattson, "Sensitivity of a Fourier transform infrared spectrometer," Appl. Spectrosc. **32,** 335–338 (1978); D. A. C. Comp-

ton, J. Drab, and H. S. Barr, "Accurate infrared transmittance measurements on optical filters using an FT-IR spectrometer," Appl. Opt. **29,** 2908–2912 (1980).
2. D. B. Chase, "Nonlinear detector response in FT-IR," Appl. Spectrosc. **38,** 491–494 (1984).
3. H. W. H. M. Jongbloets, M. J. H. Van de Steeg, E. J. C. M. Van der Werf, J. H. M. Stoelinga, and P. Wyder, "Spectrum distortion in far-infrared Fourier spectroscopy by multiple reflections between sample and Michelson interferometer," Infrared Phys. **20,** 185–192 (1980).
4. M. A. Ford, "Dispersive vs. FTIR photometric accuracy—can it be measured?" in *Advances in Standards and Methodology in Spectrophotometry*, C. Burgess and K. D. Mielenz, eds. (Elsevier, Amsterdam, 1987), pp. 359–366.
5. J. R. Birch and E. A. Nicol, "The removal of detector port radiation effects in power transmission or reflection Fourier transform spectroscopy," Infrared Phys. **27,** 159–165 (1987); D. B. Tanner and R. P. McCall, "Source of a problem with Fourier transform spectroscopy," Appl. Opt. **23,** 2363–2368 (1984).
6. J. R. Birch and F. J. J. Clarke, "Fifty categories of ordinate error in Fourier transform spectroscopy," Spectrosc. Europe **7,** 16–22 (1995).
7. J. D. Jackson, *Classical Electrodynamics* (Wiley, New York, 1975), p. 277.
8. M. I. Flik and Z. M. Zhang, "Influence of nonequivalent detector responsivity on FT-IR photometric accuracy," J. Quant. Spectrosc. Radiat. Transfer **47,** 293–303 (1992).
9. E. D. Palik, *Handbook of Optical Constants of Solids* (Academic, Orlando, Fla., 1985), p. 566.
10. H. W. Icenogle, B. C. Platt, and W. L. Wolfe, "Refractive indexes and temperature coefficients of germanium and silicon," Appl. Opt. **15,** 2348–2351 (1976); W. Primak, "Refractive index of silicon," Appl. Opt. **10,** 759–763 (1971); C. D. Salzberg and J. J. Villa, "Infrared refractive indices of silicon, germanium, and modified selenium glass," J. Opt. Soc. Am. **47,** 244–246 (1957).
11. D. F. Edwards and E. Ochoa, "Infrared refractive index of silicon," Appl. Opt. **19,** 4130–4131 (1980).
12. A. Frenkel and Z. M. Zhang, "Broadband high-optical-density filters in the infrared," Opt. Lett. **19,** 1495–1497 (1994).
13. A. L. Migdall, B. Roop, Y. C. Zheng, J. E. Hardis, and G. J. Xia, "Use of heterodyne detection to measure optical transmittance over a wide range," Appl. Opt. **29,** 5136–5144 (1990).
14. B. N. Taylor and C. E. Kuyatt, "Guidelines for evaluating and expressing the uncertainty of NIST measurement results," NIST Tech. Note 1297 (U.S. GPO, Washington, DC, 1994).
15. Z. M. Zhang, L. M. Hanssen, and R. U. Datla, "High-optical-density out-of-band spectral transmittance measurements of bandpass filters," Opt. Lett. **20,** 1077–1079 (1995).
16. K. D. Mielenz, "Physical parameters in high-accuracy spectrophotometry," Natl. Bur. Stand. (U.S.) Spec. Publ. 378 (U.S. GPO, Washington, DC, 1973).
17. Z. M. Zhang, C. J. Zhu, and L. M. Hanssen, "Methods for correcting nonlinearity errors in Fourier transform infrared spectrometers," Appl. Spectrosc. **51,** 576–579 (1997).